Supporting information for

Synthesis of highly fluorescent P, O-g-C_3N_4 nanodots for the label-free detection of Cu^{2+} and acetylcholinesterase activity

Mingcong Rong[a], Xinhong Song[a], Tingting Zhao[c], Qiuhong Yao[c], Yiru Wang[a], Xi Chen[a,b]*

[a]Department of Chemistry and the MOE Key Laboratory of Spectrochemical Analysis & Instrumentation, College of Chemistry and Chemical Engineering, Xiamen University, Xiamen 361005, China

[b]State Key Laboratory of Marine Environmental Science, Xiamen University, Xiamen, 361005, China

[c]Xiamen Huaxia University, Xiamen, 361005, China

Fluorescence quantum yield (QY) measurements

The relative QY of phosphorus, oxygen-doped graphitic carbon nitride nanodots (P, O-g-C_3N_4 nanodots) was determined with reference to quinine sulfate (QY=54% in 0.1 M H_2SO_4).[1] The same excitation and emission slit band widths were applied for both samples, and the QY for the P, O-g-C_3N_4 nanodots was calculated using the following formula:

$$QY = QY_R \bullet \frac{I}{I_R} \bullet \frac{A_R}{A} \bullet \frac{n^2}{n_R^2}$$

where the subscript "R" refers to the referenced fluorescence dye of known QY; n represents the refractive index (1.33 for both water and 0.1 M H_2SO_4); and A is the absorption at the excitation wavelength; and I is the integrated intensity (area) of the testing sample. To avoid the self-absorption effect, absorption in a 10 mm absorption cell was maintained below 0.1 at the excitation wavelength (350 nm for quinine sulfate). The QY of the P, O-g-C_3N_4 nanodots was measured to be 90.2% using this equation.

* Corresponding author. Tel: +86 592 2184530; Fax: +86 592 2184530; E-mail address: *xichen@xmu.edu.cn*

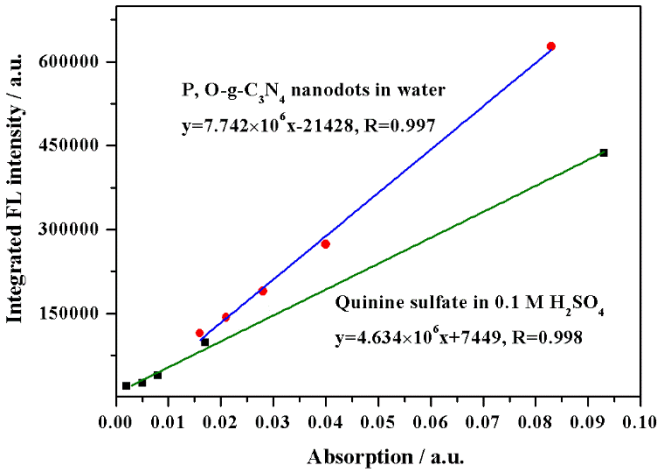

Figure S1. Plot of integrated FL intensity of the P, O-g-C_3N_4 nanodots and quinine sulfate as a function of optical absorption at 350 nm.

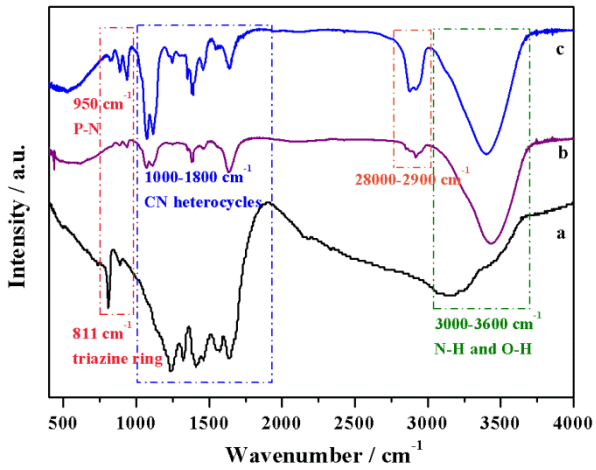

Figure S2. FT-IR spectrum of (a) the bulk P-g-C_3N_4, (b) the P, O-g-C_3N_4 nanodots and (c) P, O-g-C_3N_4 nanodots with 5 μM Cu^{2+}.

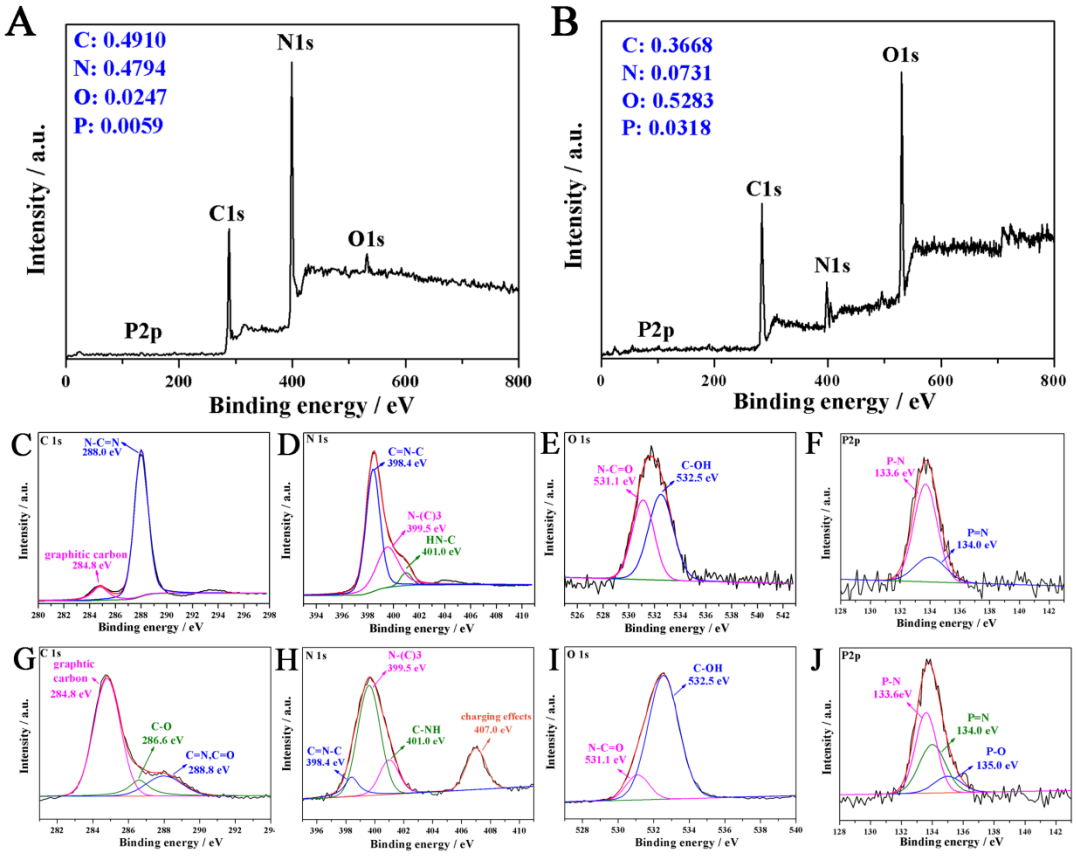

Figure S3. (A) XPS spectrum of the bulk P-g-C_3N_4. (B) XPS spectrum of the P, O-g-C_3N_4 nanodots. (C) C1s spectrum of the bulk P-g-C_3N_4. (D) N1s spectrum of the bulk P-g-C_3N_4. (E) O1s spectrum of the bulk P-g-C_3N_4. (F) P2p spectrum of the bulk P-g-C_3N_4. (G) C1s spectrum of the P, O-g-C_3N_4 nanodots. (H) N1s spectrum of the P, O-g-C_3N_4 nanodots. (I) O1s spectrum of the P, O-g-C_3N_4 nanodots. (J) P2p spectrum of the P, O-g-C_3N_4 nanodots.

Table S1. The elemental analysis results of the bulk P-g-C_3N_4 and P, O-g-C_3N_4 nanodots

Materials	N (%)	C (%)	H (%)	Other elements (%)	N/C ratio
Bulk P-g-C_3N_4	57.80	31.93	1.971	8.299	1.55
P, O-g-C_3N_4 nanodots	22.04	15.09	4.465	58.405	1.46

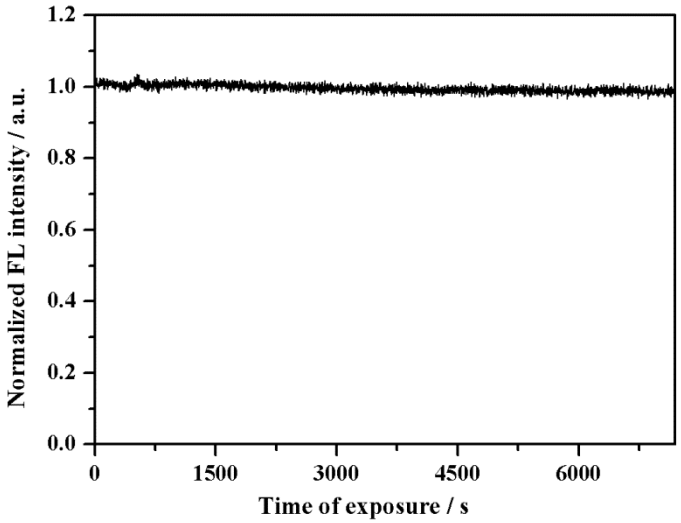

Figure S4. The photostability of the P, O-g-C_3N_4 nanodots (with excitation and emission slit: 10 nm, 10 nm, λ_{ex} = 350 nm).

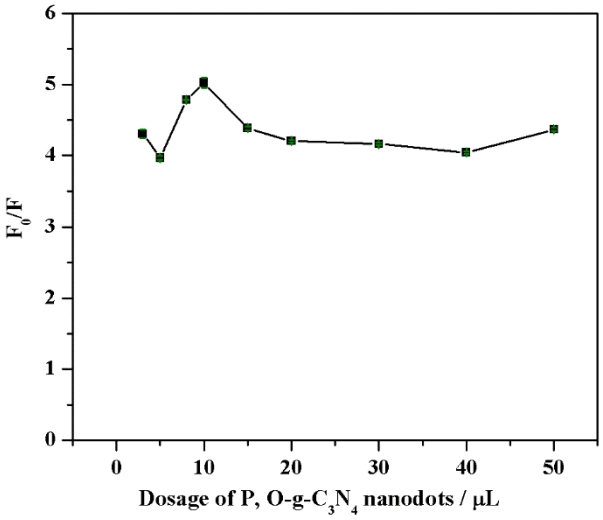

Figure S5. Relationship between the concentration of the P, O-g-C_3N_4 nanodots and the fluorescence intensity. F_0 and F represent the fluorescence of the P, O-g-C_3N_4 nanodots in the absence and presence of 3 μM Cu^{2+}.

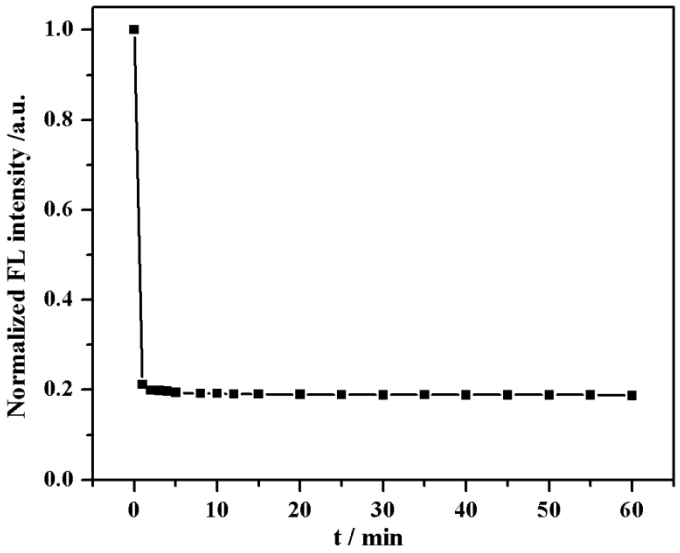

Figure S6. Kinetic characteristic of the fluorescence response of the P, O-g-C_3N_4 nanodots to 3 μM Cu^{2+} in 10 mM borate buffer (pH 7.0).

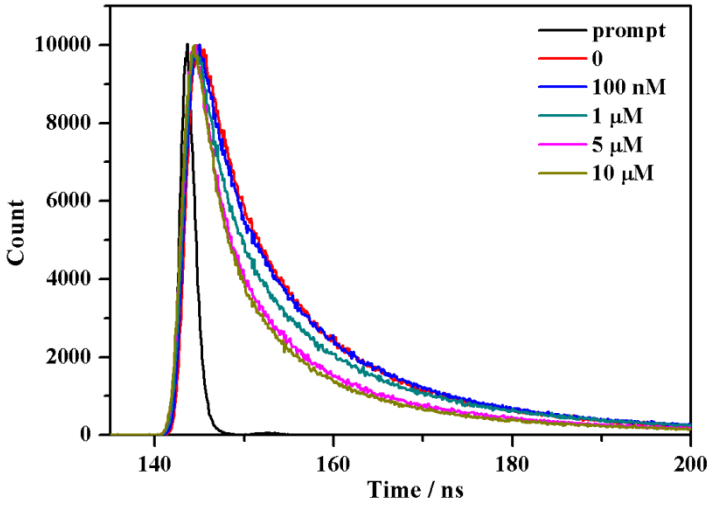

Concentration of Cu^{2+}	B_1/%	τ_1/ns	B_2/%	τ_2/ns	B_3/%	τ_3/ns	τ_{avg}/ns	χ^2
0	6.30	1.087	55.45	4.722	38.24	11.79	7.196	1.15
0.1 μM	6.02	1.068	56.86	4.683	37.12	11.89	7.139	1.07
1 μM	9.18	0.621	42.97	3.577	47.85	11.15	6.931	0.978
5 μM	12.97	0.904	49.43	4.056	37.60	12.38	6.775	1.13
10 μM	14.29	1.115	54.13	4.244	31.58	13.41	6.691	1.09

Figure S7. Time-resolved decay of the P, O-g-C_3N_4 nanodots with different concentrations of Cu^{2+} in 10 mM borate buffer (pH 7.0) and the corresponding lifetime values.

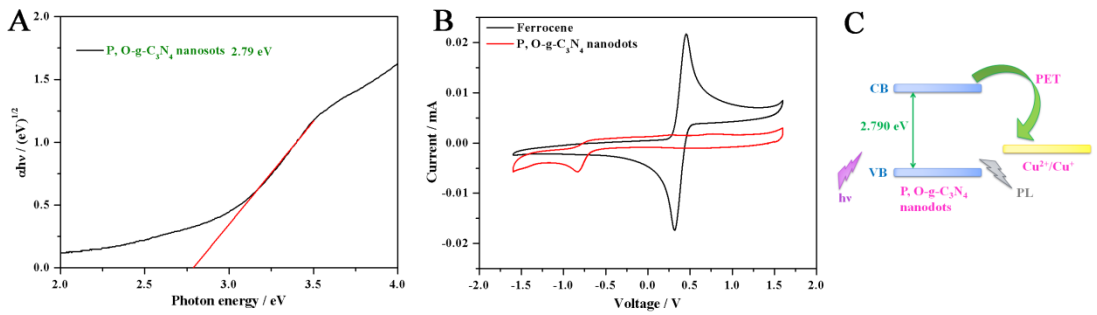

Figure S8. (A) The plots of the $(\alpha h\nu)^{1/2}$ versus photon energy. (B) Cyclic voltammogram (CV) of a glass carbon electrode (GCE) modified with the P, O-g-C_3N_4 nanodots in a de-oxygenized acetonitrile solution containing 0.1 M tetra-n-butylammonium hexafluorophosphate. (C) Schematic illustration of the PET mechanism between the P, O-g-C_3N_4 nanodots and Cu^{2+}.

The band gap of the P, O-g-C_3N_4 nanodots was determined by plotting the $(\alpha h\nu)^{1/2}$ versus photon energy from the absorption spectrum. α, h and ν are absorption coefficient, plank constant and light frequency. The extrapolating the linear region to zero on an abscissas axis is the band gap of the P, O-g-C_3N_4 nanodots ($\Delta E = 2.790$ eV).[2]

The P, O-g-C_3N_4 nanodots stock solution were mixed with 5% Nafion and then drop-casted onto the GCE. The CV were carried out in three-electrode system, with GCE as the working electrode (WE), platinum electrode as the counter electrode (CE) and saturated calomel electrode (SCE) as the reference electrode (RE). The electrode potential of SCE is 0.241 V versus normal hydrogen electrode (NHE). And the electrode potential of NHE is 4.5 V lower than the vacuum electron standard electrode potential. The valence band (VB) and conduction band (CB) were indirectly detected by HOMO and LUMO of the P, O-g-C_3N_4 nanodots by the following formulas.[3] E_{ox}^{onset} and E_{red}^{onset} are the onset oxidation and reduction potential of the P, O-g-C_3N_4 nanodots, the E_{red}^{onset} is -0.686 V according to the above figure, but the E_{ox}^{onset} is not obvious in the CV determination. $E_{ferrocene}^{1/2}$ is the average between the oxidation and reduction potential of ferrocene (measured as (0.464 + 0.329) / 2 V = 0.397 V)

$HOMO = -[E_{ox}^{onset} - E_{ferrocene}^{1/2} + 4.5 + 0.241]$ eV

$LUMO = -[E_{red}^{onset} - E_{ferrocene}^{1/2} + 4.5 + 0.241]$ eV

So, the LUMO = -[-0.686 – 0.397 + 4.5 + 0.241] eV = -3.658 eV (versus the vacuum electron standard electrode potential), the corresponding VB is 0.842 V (versus the NHE)

$\Delta E = 2.790$ eV = LUMO – HOMO

The HOMO = (-3.658 – 2.790)eV = -6.448 eV, and the corresponding CB is -1.948 V. The electrode potential of Cu^{2+}/Cu^{+} is 0.153 V (versus the NHE), so the PET mechanism may happen between the P, O-g-C_3N_4 nanodots and Cu^{2+}.

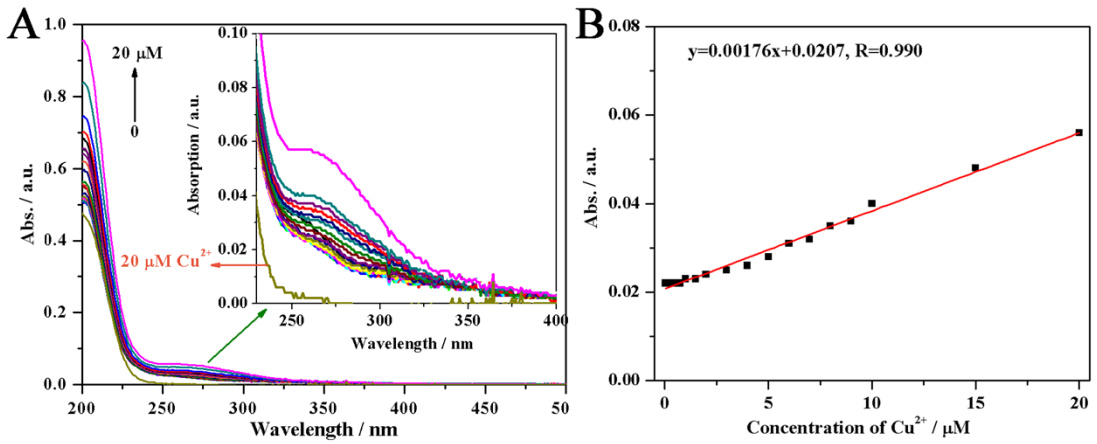

Figure S9. (A) UV-vis absorption of 20 μM Cu^{2+} aqueous and the P, O-g-C_3N_4 nanodots in the presence of increasing concentrations of Cu^{2+} in 10 mM borate buffer (pH 7.0). The inset figure presents the amplification figure of the UV-vis absorption from 230 to 400 nm. (B) The relationship between the absorbance of the P, O-g-C_3N_4 nanodots and the concentration of Cu^{2+}.

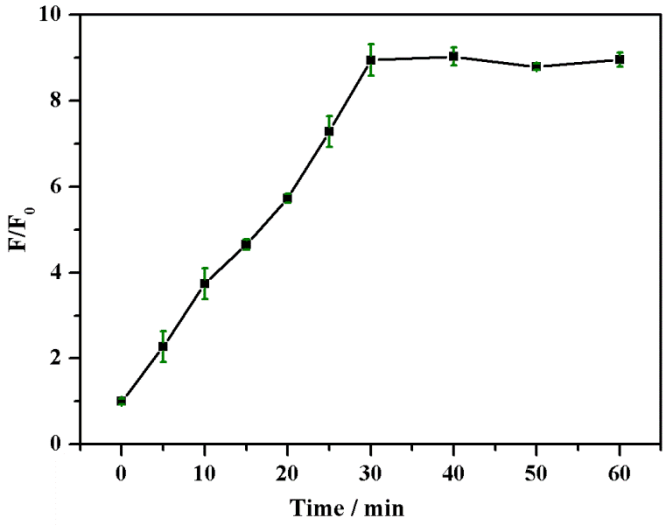

Figure S10. Fluorescence responses of the P, O-g-C_3N_4 nanodots-Cu^{2+} to 10 mU/mL AChE at different incubation times.

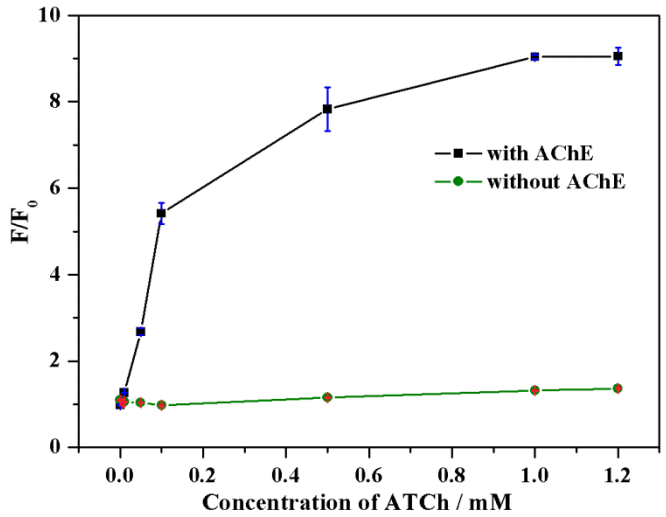

Figure S11. Fluorescence responses of the P, O-g-C_3N_4 nanodots in the absence and presence of 10 mU/mL AChE at various concentrations of ATCh.

Table S2. The comparison of different fluorescence methods for the determination of Cu^{2+}

Methods	Time consumption	Linear detection range	Detection limit	Reference
g-C_3N_4 nanosheets	10 min	0-10 nM (log)	0.5 nM	4
g-C_3N_4 nanodots	10 min	/	0.5 nM	5
CdSe/ZnS QDs	/	0-0.6 μM	0.14 nM	6
Au-AgNCs	5 min	0.5-2.5 μM (log)	0.3 nM	7
H_{39}GFP fluorescent protein	5 min	0.05-2 μM	50 nM	8
Carbon quantum dots	1 min	1-100 μM	10 nM	9
Carbon quantum dots	/	2-80 nM	1.8 nM	10
Europium complex-functionalized magnetic nanoparticle	5 min	0.1-1 nM	0.1 nM	11
Iridium(III) complex	/	0.1-80 μM	22.6 nM	12
P, O-g-C_3N_4 nanodots	5 min	0-1 μM	2 nM	This work

Table S3. The comparison of different fluorescence methods for the determination of AChE activity

Methods	Incubation time consumption	Linear detection range	Detection limit	Reference
DNA-Cu/AgNCs	20 min	0.05-2 mU/mL	0.05 mU/mL	13
FITC/BSA-AuNCs	30 min	0.8-12 mU/mL	0.4 mU/mL	14
Ag@SiO_2 nanoparticles	/	0-5 mU/mL	0.05 mU/mL	15
Carbon dots	10 min	1-80 mU/mL	/	16
H_{39}GFP fluorescent protein	30 min	0.025-2 mU/mL	0.015 mU/mL	8
Graphene quantum dots	25 min	/	2.3 mU	17
AuNCs@11-MUA-Cu^{2+}	20 min	0.05-2.5 mU/mL	0.05 mU/mL	18
P, O-g-C_3N_4 nanodots	30 min	0.01-3 mU/mL	0.01 mU/mL	This work

References

1. M. Rong, L. Lin, X. Song, T. Zhao, Y. Zhong, J. Yan, Y. Wang and X. Chen, *Anal. Chem.*, 2015, 87, 1288-1296.
2. J. Ye, Y. Li, H. Xu, S. Ouyang, D. Lu, X. Wang and D. Wang, *J. Mater. Chem. A*, 2015, DOI: 10.1039/c5ta05128b.
3. A. Ananthanarayanan, X. W. Wang, P. Routh, B. Sana, S. Lim, D. H. Kim, K. H. Lim, J. Li and P. Chen, *Adv. Funct. Mater.*, 2014, 24, 3021-3026.
4. J. Tian, Q. Liu, A. M. Asiri, A. O. Al-Youbi and X. Sun, *Anal. Chem.*, 2013, 85, 5595-5599.
5. S. Zhang, J. Li, M. Zeng, J. Xu, X. Wang and W. Hu, *Nanoscale*, 2014, 6, 4157-4162.
6. L. H. Jin and C. S. Han, *Anal. Chem.*, 2014, 86, 7209-7213.
7. N. Zhang, Y. Si, Z. Sun, L. Chen, R. Li, Y. Qiao and H. Wang, *Anal. Chem.*, 2014, 86, 11714-11721.
8. C. Lei, Z. Wang, Z. Nie, H. Deng, H. Hu, Y. Huang and S. Yao, *Anal. Chem.*, 2015, 87, 1974-1980.
9. Q. Qu, A. Zhu, X. Shao, G. Shi and Y. Tian, *Chem Commun*, 2012, 48, 5473-5475.
10. M. Vedamalai, A. P. Periasamy, C. W. Wang, Y. T. Tseng, L. C. Ho, C. C. Shih and H. T. Chang, *Nanoscale*, 2014, 6, 13119-13125.
11. J. Liu, W. Zuo, W. Zhang, Z. Wang, Z. Yang and B. Wang, *Nanoscale*, 2014, 6, 11473-11478.
12. D. L. Ma, H. Z. He, D. S. Chan, C. Y. Wong and C. H. Leung, *PloS one*, 2014, 9, e99930-e99937.
13. W. Li, Y. Hu, Y. Xia, Q. Shen, Z. Nie, Y. Huang and S. Yao, *Biosens. Bioelectron.*, 2013, 47, 345-349.
14. C. Y. Ke, Y. T. Wu and W. L. Tseng, *Biosens. Bioelectron.*, 2015, 69C, 46-53.
15. K. Ma, L. Lu, Z. Qi, J. Feng, C. Zhuo and Y. Zhang, *Biosens. Bioelectron.*, 2015, 68, 648-653.
16. X. Ren, J. Wei, J. Ren, L. Qiang, F. Tang and X. Meng, *Colloids Surf., B*, 2015, 125, 90-95.
17. T. He, L. Qi, J. Zhang, Y.-L. Huang and Z.-Q. Zhang, *Sens. Actuators, B*, 2015, 215, 24-29.
18. J. Sun and X. Yang, *Biosens. Bioelectron.*, 2015, **74**, 177-182.